Auxin transport-feedback models of patterning in plants

Smith, R S ; Bayer, E M

DOI: https://doi.org/10.1111/j.1365-3040.2009.01997.x

Supplemental Materials – Simulation details

All simulations shown in the figures in the main text are modeled as coupled systems of ordinary differential equations that are solved numerically using the forward Euler method. Cells are represented by single compartments, with the cell-to-cell connections abstracted to singles interfaces ignoring extra-cellular space. In the simulations performed on a line or grid of cells, the cells are considered to have unit volume with walls of unit length. In the growing leaf simulation with irregularly shaped cells depicted in Fig. 6, the volume of cells and length of cell-to-cell interfaces is taken into account.

Simulations depicted in Figure 2

The simulations shown in Figure 2 were performed on a line of cells connected at the ends to form a ring (wraparound boundary conditions). This is one of the topologies originally considered by Turing (1952) and is perhaps the simplest multicellular system that gives group of identical cells

Figure 2A was generated using a variation of the activator-inhibitor model proposed by Gierer and Meinhardt (1972). The equations for the change in concentration of the activator and the inhibitor are as follows:

$$\frac{da_i}{dt} = \rho_{a_0} + \rho_a \frac{a_i^{\,2}}{1+h_i} - \mu_a a_i - D_a \sum_{j \in N_i} \left(a_i - a_j\right) \qquad (1)$$

$$\frac{dh_i}{dt} = \rho_{h_0} + \rho_h a_i^{\,2} - \mu_h a_i - D_h \sum_{j \in N_i} \left(h_i - h_j\right) \qquad (2)$$

Noise is added to the activator production term in order to break the symmetry of the system. The variables and parameters for equations (1-2) are defined as follows:

Symbol	Description	Value
a_i	activator concentration in cell *i*	variable
ρ_{a_0}	background activator production coefficient	.01
ρ_a	activator dependant activator production coefficient	10
μ_a	activator decay coefficient	.1
D_a	activator diffusion coefficient	.01
N_i	neighbors of cell *i*	variable
h_i	inhibitor concentration in cell *i*	variable
ρ_{h_0}	background inhibitor production coefficient	0
ρ_h	activator dependant inhibitor production coefficient	50
μ_h	inhibitor decay coefficient	.5
D_h	inhibitor diffusion coefficient	2

Figure 2B was generated using the equations for auxin (IAA) dynamics and PIN polarization after the phyllotaxis models presented in Smith et al. (2006) as follows:

$$\frac{d\,PIN_i}{dt} = \rho_{PIN}\frac{IAA_i}{1+PIN_i} - \mu_{PIN}PIN_i \tag{3}$$

$$PIN_{i\to j} = PIN_i\frac{b^{IAA_i}}{\sum_{k\in N_i} b^{IAA_k}} \tag{4}$$

$$\begin{aligned}\frac{d\,IAA_i}{dt} = {} & \frac{\rho_{IAA}}{1+IAA_i} - \mu_{IAA}IAA_i - D_{IAA}\sum_{j\in N_i}\left(IAA_i - IAA_j\right) \\ & - T_{IAA}\sum_{j\in N_i}\left(PIN_{i\to j}\frac{IAA_i^{\,2}}{1+IAA_j^{\,2}} - PIN_{j\to i}\frac{IAA_j^{\,2}}{1+IAA_i^{\,2}}\right)\end{aligned} \tag{5}$$

Noise is added to the IAA production term in order to break the symmetry of the system. The variables and parameters for equations (3-5) are defined as follows:

Symbol	Description	Value
PIN_i	total amount of PIN in cell *i*	variable
ρ_{PIN}	PIN production coefficient	1
μ_{PIN}	PIN decay coefficient	.1
$PIN_{i\to j}$	PIN located at the membrane section of cell *i* facing cell *j*	variable
b	base for exponential PIN allocation	3
N_i	neighbors of cell *i*	variable
IAA_i	IAA concentration in cell *i*	variable
ρ_{IAA}	IAA production coefficient	2
μ_{IAA}	IAA decay coefficient	.1
D_{IAA}	IAA diffusion coefficient	0.01
T_{IAA}	IAA transport coefficient	2

Figure 2C uses the upregulation of import proteins (AUX), and their subsequent effect on increasing transport to activate cells and create a pattern. Since the polarity and overall amount of the exporter proteins (PIN) remain constant throughout the simulation, their dynamics are not modeled and are accounted for in the transport coefficient. The auxin and import protein dynamics are modeled as follows:

$$\frac{d\,AUX_i}{dt} = \frac{\rho_{AUX_0} + \rho_{AUX}IAA_i^{\,2}}{\kappa_{AUX} + AUX_i^{\,2}} - \mu_{AUX}AUX_i \tag{6}$$

$$\frac{d\,IAA_i}{dt} = \rho_{IAA} - \mu_{IAA} IAA_i - D_{IAA} \sum_{j \in N_i} \left(IAA_i - IAA_j \right) - T_{IAA} \sum_{j \in N_i} \left(AUX_j \frac{IAA_i}{\kappa_T + IAA_j} - AUX_i \frac{IAA_j}{\kappa_T + IAA_i} \right) \quad (7)$$

Noise is added to the IAA production term in order to break the symmetry of the system. Note the quadratic dependence of AUX on IAA concentration, as well as the saturation of both AUX production and IAA transport. The variables and parameters for equations (6-7) are defined as follows:

Symbol	Description	Value
AUX_i	total amount of AUX in cell *i*	variable
ρ_{AUX_0}	AUX background production coefficient	.01
ρ_{AUX}	IAA dependant AUX production coefficient	1000
κ_{AUX}	AUX production saturation coefficient	100
μ_{AUX}	AUX decay coefficient	.1
N_i	neighbors of cell *i*	variable
IAA_i	IAA concentration in cell *i*	variable
ρ_{IAA}	IAA production coefficient	.01
μ_{IAA}	IAA decay coefficient	.1
D_{IAA}	IAA diffusion coefficient	.7
T_{IAA}	IAA transport coefficient	500
κ_{IAA}	IAA production saturation coefficient	100

Simulation depicted in Figure 4

The simulation shown in Figure 4 was a reproduction of the simulation presented in Fig. 3d of Feugier et al. (2005). The simulation differs from the original in that a rectangular rather than a hexagonal grid was used, and auxin production was increased by raising the threshold for the shutdown of auxin production. The increased production likely reflects the change in topology as well as the reduced number of cells in the simulation. The equations for auxin and PIN dynamics are as follows:

$$\begin{aligned} \frac{d\,S_i}{dt} &= s\left[1 - \frac{IAA_i}{IAA_{eq}}\right] - \delta S_i \qquad if \quad \left[1 - \frac{IAA_i}{IAA_{eq}}\right] > 0 \\ \frac{d\,S_i}{dt} &= -\delta S_i \qquad\qquad\qquad if \quad \left[1 - \frac{IAA_i}{IAA_{eq}}\right] \le 0 \end{aligned} \quad (8)$$

$$J_{i\to j} = \frac{1}{2}\alpha\left(IAA_i PIN_{i\to j} - IAA_j PIN_{j\to i}\right) \tag{9}$$

$$\varphi(J) = \frac{a J^2}{1+J} \qquad if\ J>0$$
$$\varphi(J) = 0 \qquad if\ J\le 0 \tag{10}$$

$$\frac{d\,PIN_{i\to j}}{dt} = \lambda\left(\Psi_i\left(\varphi(J_{i\to j}) + q_a\right) - PIN_{i\to j}\right) \tag{11}$$

$$\frac{d\,\Psi_i}{dt} = -\sum_{j\in N_i}\frac{d\,PIN_{i\to j}}{dt} \tag{12}$$

$$\frac{d\,IAA_i}{dt} = \varepsilon S_i - \sum_{j\in N_i} J_{i\to j} \tag{13}$$

As in Feugier et al (2005), auxin is produced in a two step process, with equation (8) representing the dynamics of an auxin biosynthesis enzyme. The simulation uses a linear transport function (Eq. 9) and quadratic, curvilinear carrier allocation (Eq. 10) from a pool of PIN (Eq. 12). The total amount of PIN per cell is fixed. The variables and parameters for equations (8-13) are defined as follows:

Symbol	Description	Value
S_i	concentration of IAA biosynthesis enzyme in cell *i*	variable
IAA_i	IAA concentration in cell *i*	variable
IAA_{eq}	Threshold at which IAA production shuts down	2
s	IAA biosynthesis enzyme production coefficient	.18
δ	IAA biosynthesis enzyme decay coefficient	1
$J_{i\to j}$	IAA flux from cell *i* to *j*	variable
$PIN_{i\to j}$	PIN located at the membrane section of cell *i* facing cell *j*	variable
α	IAA transport coefficient	6
a	IAA flux response function coefficient	1
λ	PIN turnover coefficient	.7
Ψ_i	PIN in cytosol of cell *i* available for allocation	variable initial value 2
N_i	neighbors of cell *i*	variable
q_a	PIN flux independent allocation coefficient	.05
ε	IAA production coefficient	1

Simulations depicted in Figure 5

The simulations shown in Figure 5 are based on Mitchison's model of canalization (Mitchison 1981) and equations and parameters presented in Rolland-Lagan and Prusinkiewicz (2005). Point sources for auxin were implemented by including auxin production in source cells, and point sinks were implemented by setting sink cell concentration to zero at every timestep. Equations for the polar transport model (Fig. 5A) were as follows:

$$\phi_{i\to j} = PIN_{i\to j} IAA_i - PIN_{j\to i} IAA_j \tag{14}$$

$$\begin{aligned} \frac{d\,PIN_{i\to j}}{dt} &= \alpha \phi_{i\to j}{}^2 + \beta - \gamma\, PIN_{i\to j} \qquad if\ \phi_{i\to j} > 0 \\ \frac{d\,PIN_{i\to j}}{dt} &= \beta - \gamma\, PIN_{i\to j} \qquad if\ \phi_{i\to j} \le 0 \end{aligned} \tag{15}$$

$$\frac{d\,IAA_i}{dt} = \rho - \sum_{j\in N_i} \phi_{i\to j} \tag{16}$$

The variables and parameters for equations (14-16) are as follows:

Symbol	Description	Value
$\phi_{i\to j}$	flux from cell *i* to *j*	variable
$PIN_{i\to j}$	PIN located at the membrane section of cell *i* facing cell *j*	variable initial value .325
α	PIN production/allocation based on flux	.00005
β	flux independent PIN production/allocation	.005
γ	PIN decay coefficient	.1
N_i	neighbors of cell *i*	variable
IAA_i	IAA concentration in cell *i*	variable
ρ	IAA production coefficient (source cell only)	30

Equations for the facilitated diffusion model (Fig. 5B) were as follows:

$$\phi_{i\to j} = \tilde{D}_{ij}\left(IAA_i - IAA_j\right) \tag{17}$$

$$\frac{d\tilde{D}_{ij}}{dt} = \alpha \phi_{i\to j}{}^2 + \beta - \gamma \tilde{D}_{ij} \tag{18}$$

$$\frac{d\,IAA_i}{dt} = \rho - \sum_{j\in N_i} \phi_{i\to j} \tag{19}$$

Note that the diffusion constant is symmetrical, that is $\tilde{D}_{ij} = \tilde{D}_{ji}$ and because of the quadratic term in equation (18) it does not matter which direction is used for the flux. The variables and parameters for equations (17-19) are as follows:

Symbol	Description	Value
$\phi_{i\to j}$	flux from cell *i* to *j*	variable
$\tilde{D}_{ij}$	diffusion coefficient between cells *i* and *j*	variable initial value .325
α	channel production/allocation based on flux	.00005
β	flux independent channel production/allocation	.005
γ	channel decay coefficient	.1
N_i	neighbors of cell *i*	variable
IAA_i	IAA concentration in cell *i*	variable
ρ	IAA production coefficient in source cells	70

Simulation depicted in Figure 6

The simulation in Figure 6 combines the canalization model for leaf venation with the transport-feedback model proposed for phyllotaxis (Jönsson, Heisler et al. 2006; Smith, Guyomarc'h et al. 2006). Cells in the leaf margin use equations adapted from Smith et al. (2006), whereas interior cells use Mitchison's canalization model (Mitchison 1981; Rolland-Lagan and Prusinkiewicz 2005). Up-the-gradient polarization in margin cells causes convergence points to appear, and when the auxin concentration in the center cells of these convergence points reaches a threshold, they differentiate and become auxin sources, and auxin begins to leak into inner tissue. Canalization (with-the-flux polarization) in interior cells causes strands to appear in the interior of the leaf. As the leaf grows and more space opens up in the margin, more convergence points form, leading to the initiation of more veins.

The equations for the up-the-gradient transport-feedback model used in margin cells were as follows:

$$\frac{d\,PIN_i}{dt} = \frac{\rho_{PIN}}{1+PIN_i} - \mu_{PIN} PIN_i \tag{20}$$

$$IAA_i' = \max\left\{ IAA_i, IAA_{th}\left(1-\frac{d_i}{r}\right)\right\} \tag{21}$$

$$PIN_{i\to j} = PIN_i \frac{l_{i\to j} b_{PIN}{}^{IAA_j'}}{\sum_{k\in N_i} l_{i\to k} b_{PIN}{}^{IAA_k'}} \tag{22}$$

$$\begin{aligned}\frac{d\,IAA_i}{dt} = {} & \frac{\rho_{IAA} + \rho_{src}\left(1-\frac{d_i}{r}\right)_+}{1+IAA_i} - \mu_{IAA} IAA_i - \frac{D_{IAA}}{A_i}\sum_{j\in N_i} l_{i\to j}\left(IAA_i - IAA_j\right) \\ & - \frac{T_{IAA}}{A_i}\sum_{j\in N_i}\left(PIN_{i\to j}\frac{IAA_i{}^2}{1+IAA_j{}^2} - PIN_{j\to i}\frac{IAA_j{}^2}{1+IAA_i{}^2}\right)\end{aligned} \tag{23}$$

The + sign in equation (23) indicates that the term $\left(1-\frac{d_i}{r}\right)_+$ is used only if it is positive; otherwise it is 0. Thus there is no source production at a distance greater than r from the center of sources. The variables and parameters for equations (20-23) are as follows:

Symbol	Description	Value
PIN_i	total amount of PIN in cell i	variable
ρ_{PIN}	PIN production coefficient	.1
μ_{PIN}	PIN decay coefficient	.1
$PIN_{i\to j}$	PIN located at the membrane section of cell i facing cell j	variable
$l_{i\to j}$	length of interface between cell i and j	variable
A_i	area of cell i	variable
b	base for exponential PIN allocation	3
N_i	neighbors of cell i	variable
IAA_i	IAA concentration in cell i	variable
IAA_i'	IAA effective concentration in sources	variable
IAA_{th}	IAA threshold for source differentiation	7
ρ_{IAA}	IAA production coefficient	10
ρ_{src}	IAA additional production in sources	30
μ_{IAA}	IAA decay coefficient	0
D_{IAA}	IAA diffusion coefficient	2
T_{IAA}	IAA transport coefficient	60
d_i	distance from cell center to source center	variable
r	radius of influence of sources	3

The equations for the canalization model used in interior leaf cells were as follows:

$$\phi_{i\to j} = T_{IAA}\left(PIN_{i\to j}\frac{IAA_i^{\,2}}{1+IAA_j^{\,2}} - PIN_{j\to i}\frac{IAA_j^{\,2}}{1+IAA_i^{\,2}}\right) + D_{IAA}\left(IAA_i - IAA_j\right) \qquad (24)$$

$$\begin{aligned} \frac{d\,PIN_{i\to j}}{dt} &= \alpha\,\phi_{i\to j}^{\,2} + \beta - \gamma\,PIN_{i\to j} && \text{if } \phi_{i\to j} > 0 \\ \frac{d\,PIN_{i\to j}}{dt} &= \beta - \gamma\,PIN_{i\to j} && \text{if } \phi_{i\to j} \le 0 \end{aligned} \qquad (25)$$

$$\frac{d\,IAA_i}{dt} = \frac{\rho}{1+IAA_i} - \mu\,IAA_i - \frac{1}{A_i}\sum_{j\in N_i} l_{i\to j}\phi_{i\to j} \qquad (26)$$

The variables and parameters for equations (24-26) are as follows:

Symbol	Description	Value
$\phi_{i\to j}$	flux from cell *i* to *j*	variable
$PIN_{i\to j}$	PIN located at the membrane section of cell *i* facing cell *j*	variable
α	PIN production/allocation based on flux	3
β	flux independent PIN production/allocation	0
γ	PIN decay coefficient	.1
N_i	neighbors of cell *i*	variable
$l_{i\to j}$	length of interface between cell *i* and *j*	variable
A_i	area of cell *i*	variable
IAA_i	IAA concentration in cell *i*	variable
D_{IAA}	IAA diffusion coefficient	2
T_{IAA}	IAA transport coefficient	60
ρ	IAA production coefficient (source cell only)	30
μ	IAA decay coefficient	0

Growing cellular leaf surface

The growing leaf was implemented by defining a sequence of Bezier surfaces that represent the leaf at different times (key frames) during the simulation (Fig. S1). These surfaces are defined using the Bezier surface editor provided with L-studio (Prusinkiewicz 2004), which allows the user to specify the control points of the surface interactively. Linear interpolation of the control points of the surfaces is used to produce the leaf at any desired point between the key frames. By advancing time in small steps, a smoothly growing leaf surface is produced. The Bezier surfaces used to model the leaf are two-dimensional parametric surfaces embedded in three-dimensional space. Points on the surface are represented by two-dimensional coordinates (u, v) which are mapped by Bezier surface evaluators to positions (x, y, z). As the leaf changes shape, a (u, v) coordinate at the tip of the leaf will remain at the tip even though its actual position in space might change considerably (Fig. S1).

The same dividing cellular structure used to model phyllotaxis and described in Smith et al. (2006) was implemented on the growing leaf. The simulation starts with a single initial cell that covers the entire surface, which is then subdivided until all cells are below a threshold area. Cells are divided by choosing the shortest wall that passes through the center, and then pinching them a small amount to help keep them convex (see Smith et al (2006) for further details). As the simulation proceeds, the leaf grows causing the cells to enlarge, which are again divided when they reach the threshold area. The program library that implements the Bezier surface has two main functions; one to compute the (x, y, z) coordinates of a point on the surface given its (u, v) coordinates, and the other to perform the inverse operation. The evaluator used to compute the (x, y, z) coordinates was programmed from the equations given in Neider et al. (1994), however in general there is no closed formula to compute the (u, v) coordinate given a particular (x, y, z) position that may or may not be on the surface. This inverse operation is required whenever new points are added to the model, such as during cell division, and is implemented by using a steepest decent search algorithm on the evaluator function.

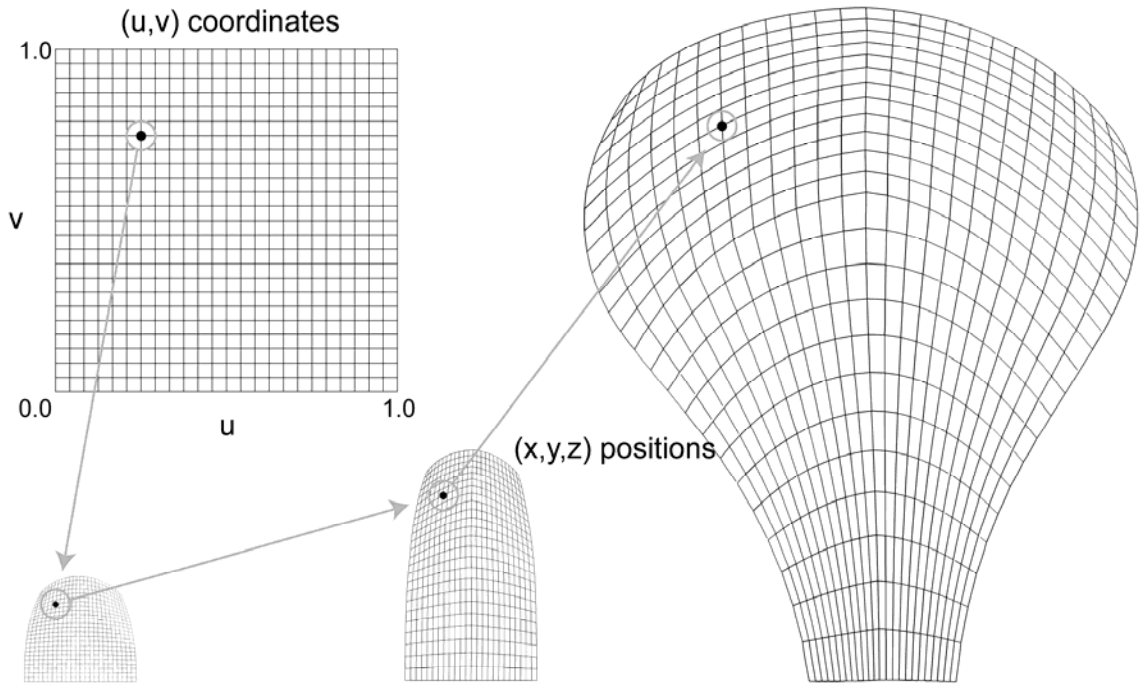

Figure S1. Modeling a growing leaf by using Bezier surfaces. A sequence of Bezier surfaces represents the leaf at various times (key frames) during the simulation. Coordinates in the parameter space (u, v) shown in the top left are mapped into three-dimensional space (x, y, z) as shown. The position of points at time steps in between the three key frames is found by linear interpolation between the key frames.

General

All simulations were programmed in C++ using OpenGL, QT4, and the VV simulation tool (Smith 2004) under the L-studio modeling environment (Prusinkiewicz 2004).

Bibliography

Feugier, F. G., A. Mochizuki, et al. (2005). "Self-organization of the vascular system in plant leaves: inter-dependent dynamics of auxin flux and carrier proteins." Journal of Theoretical Biology 236(4): 366-375.

Gierer, A. and H. Meinhardt (1972). "A theory of biological pattern formation." Kybernetik 12(1): 30-39.

Jönsson, H., M. Heisler, et al. (2006). "An auxin-driven polarized transport model for phyllotaxis." Proceedings of the National Academy of Science of the USA.

Mitchison, G. J. (1981). "The polar transport of auxin and vein patterns in plants." Philosophical Transactions of the Royal Society of London. B. Biological Sciences 295: 461-271.

Neider, J. D., Tom & Woo, Mason (1994). OpenGL Programming Guide 9 (The Red Book), Addison-Wesley.

Prusinkiewicz, P. (2004). "Art and Science for Life: Designing and Growing Virtual Plants with L-systems." Acta Hortic 630: 15–28.

Rolland-Lagan, A. G. and P. Prusinkiewicz (2005). "Reviewing models of auxin canalization in the context of leaf vein pattern formation in Arabidopsis." The Plant Journal 44(5): 854-865.

Smith, C. P., Przemyslaw & Samavati, Faramarz (2004). Local specification of surface subdivision algorithms. Applications of Graph Transformations with Industrial Relevance: Second International Workshop, AGTIVE 2003, Springer-Verlag GmbH.

Smith, R. S., S. Guyomarc'h, et al. (2006). "A plausible model of phyllotaxis." Proceedings of the National Academy of Science of the USA 103(5): 1301--1306.

Turing, A. M. (1952). "The chemical basis of morphogenesis." Philosophical Transactions of the Royal Society of London. B. Biological Sciences 237: 37-52.